endo-Hydroxamic Acid Monomers for the Assembly of a Suite of Non-native Dimeric Macrocyclic Siderophores Using Metal-Templated Synthesis

Brown, Christopher J M ; Gotsbacher, Michael P ; Holland, Jason P ; Codd, Rachel

Abstract: An expedited synthesis of endo-hydroxamic acid aminocarboxylic acid (endo-HXA) compounds has been developed. These monomeric ligands are relevant to the synthesis of metal–macrocycle complexes using metal-templated synthesis (MTS), and the downstream production of apomacrocycles. Macrocycles can display useful drug properties and be used as ligands for radiometals in medical imaging applications, which supports methodological advances in accessing this class of molecule. Six endo-HXA ligands were prepared that contained methylene groups, ether atoms, or thioether atoms in different regions of the monomer (1–6). MTS using a 1:2 Fe(III)/ligand ratio furnished six dimeric hydroxamic acid macrocycles complexed with Fe(III) (1a–6a). The corresponding apomacrocycles (1b–6b) were produced upon treatment with diethylenetriaminepentaacetic acid (DTPA). Constitutional isomers of the apomacrocycles that contained one ether oxygen atom in the diamine-containing (2b) or dicarboxylic acid-containing (3b) region were well resolved by reverse-phase high-performance liquid chromatography (RP-HPLC). Density functional theory calculations were used to compute the structures and solvated molecular properties of 1b–6b and showed that the orientation of the amide bonds relative to the pseudo-C2 axis was close to parallel in 1b, 2b, and 4b–6b but tended toward perpendicular in 3b. This conformational constraint in 3b reduced the polarity compared with 2b, consistent with the experimental trend in polarity observed using RP-HPLC. The improved synthesis of endo-HXA ligands allows expanded structural diversity in MTS-derived macrocycles and the ability to modulate macrocycle properties.

DOI: https://doi.org/10.1021/acs.inorgchem.9b00878

Endo-Hydroxamic Acid Monomers for the Assembly of a Suite of Non-Native Dimeric Macrocyclic Siderophores Using Metal-Templated Synthesis

Christopher J. M. Brown[†] (ORCID: 0000-0003-2272-3720), Michael P. Gotsbacher[†] (ORCID: 0000-0002-7153-1250), Jason P. Holland[‡] (0000-0002-0066-219X), Rachel Codd*[,†] (ORCID: 0000-0002-2703-883X)

[†]School of Medical Sciences (Pharmacology), The University of Sydney, New South Wales 2006, Australia

[‡]University of Zurich, Department of Chemistry, Winterthurerstrasse 190, 8057 Zurich, Switzerland

Corresponding author. Tel.: +61 2 9351 6738.

E-mail address: rachel.codd@sydney.edu.au (R. Codd).

Keywords:

endo-Hydroxamic acids

Metal-templated synthesis

Macrocyclic siderophores

Density functional theory calculations

Abstract

An expedited synthesis of *endo*-hydroxamic acid amino carboxylic acid (*endo*-HXA) compounds has been developed. These monomeric ligands are relevant to the synthesis of metal-macrocycle complexes using metal-templated synthesis (MTS), and the downstream production of apo-macrocycles. Macrocycles can display useful drug properties and be used as ligands for radiometals in medical imaging applications, which supports methodological advances in accessing this class of molecule. Six *endo*-HXA ligands were prepared that contained methylene groups, ether atoms or thioether atoms in different regions of the monomer (**1**–**6**). MTS using a 1:2 Fe(III):ligand ratio furnished six dimeric hydroxamic acid macrocycles complexed with Fe(III) (**1a**–**6a**). The corresponding apo-macrocycles (**1b**–**6b**) were produced upon treatment with diethylenetriaminepentaacetic acid (DTPA). Constitutional isomers of the apo-macrocycles that contained one ether oxygen atom in the diamine- (**2b**) or the dicarboxylic acid- (**3b**) containing region were well resolved by reverse-phase liquid chromatography. Density functional theory (DFT) calculations used to compute the structures and solvated molecular properties of **1b**–**6b**, showed the orientation of the amide bonds relative to the pseudo C_2 axis was close to parallel in **1b**, **2b**, and **4b**–**6b**, but tended towards perpendicular in **3b**. This conformation constraint manifest in **3b** reduced the polarity compared with **2b**, and was consistent with the experimental trend in polarity observed using RP-HPLC. The improved synthesis of *endo*-HXA ligands allows expanded structural diversity in MTS-derived macrocycles and the ability to modulate macrocycle properties.

Introduction

Almost all bacteria produce low-molecular-weight organic ligands known as siderophores that have high affinity toward Fe(III).[1-4] The formation of Fe(III)-siderophore complexes occurs as the first step in siderophore-mediated bacterial iron acquisition, which serves to increase the availability of insoluble Fe(III) to bacteria, as essential for survival.[5-8] Due to evolutionary pressure, a vast array of siderophores are produced with different molecular structures.[4] A large sub-set of siderophores contain the hydroxamic acid functional group as the Fe(III) binding motif. Trimeric hydroxamic acid siderophores form hexadentate 1:1 complexes with Fe(III) and include linear desferrioxamine B (DFOB) and macrocyclic desferrioxamine E (DFOE).[9-11] Dimeric hydroxamic acid macrocyclic siderophores isolated from nature include putrebactin, avaroferrin, bisucaberin and alcaligin (Chart 1). These tetradentate macrocycles form 2:3 Fe(III):ligand complexes at pH 7 and 1:1 complexes at acidic pH values,[12-19] and can form complexes with other metal ions, including V(V), Mo(VI) and Cr(V).[16,20,21] Bisucaberin has been shown to have anti-cancer potential through Fe(III) deprivation mechanisms,[17] which provides impetus to exploring methods beyond total synthesis[22] to improve access to these types of molecules and to allow increased structural diversity. This is in accord with the broader potential of macrocycles as useful drug leads and inhibitors of protein-protein interactions,[23-28] which underpins developments in macrocycle synthesis.

Metal-templated synthesis (MTS) from *endo*-hydroxamic acid amino carboxylic acid (*endo*-HXA) monomers has been used to furnish a range of dimeric,[29] trimeric,[30,31] or tetrameric[32] hydroxamic acid macrocycles. In a different approach, trimeric macrocyclic hydroxamic acid siderophores have been produced using Fe(III)-mediated macrolactonization of a pre-assembled linear trimer.[33] Trimeric DFOE was first produced using MTS as a

supramolecular chemistry approach from a 1:3 complex formed *in situ* between Fe(III) and the *endo*-HXA monomer 4-[(5-aminopentyl)(hydroxy)amino]-4-oxobutanoic acid (PBH).[30] The flanking amino and carboxylic acid groups of contiguous PBH ligands were favourably positioned around the Fe(III) template for ring closure using diphenylphosphoryl azide (DPPA)-mediated peptide coupling. Ring-expanded analogues of trimeric DFOE were subsequently generated using MTS with the replacement of PBH with *endo*-HXA monomers that contained additional methylene groups in the diamine- or carboxylic acid-containing region of the ligand.[31] In a given MTS system, the nature of the metal ion template, the *endo*-HXA and the reaction stoichiometry can direct the architecture of the terminal macrocycle. The use of Zr(IV) (typical coordination numbers in the range 6–8)[34,35] and the *endo*-HXA 5-[(5-aminopentyl)(hydroxy)amino]-5-oxopentanoic acid (PPH) in a 1:4 ratio furnished a tetrameric hydroxamic acid macrocycle that saturated the Zr(IV) octadentate coordination sphere.[32] A selection of natural product dimeric hydroxamic acid macrocycles has been generated by MTS using a 1:2 Fe(III):ligand reaction stoichiometry.[29]

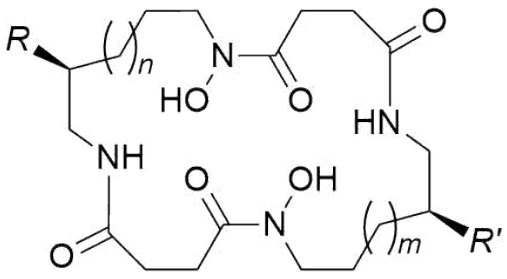

$n = m = 0$, $R = R' = H$	putrebactin
$n = 0$, $m = 1$, $R = R' = H$	avaroferrin
$n = m = 1$, $R = R' = H$	bisucaberin
$n = m = 0$, $R = R' = OH$	alcaligin

Chart 1. Dimeric hydroxamic acid macrocyclic siderophores characterized from nature.

One shortcoming of MTS in generating new macrocycles is the availability of the *endo*-HXA monomers. The existing literature syntheses[36,37] provide monomers in modest yields (about 10 mg per 5-day synthetic undertaking), which can hinder progress in exploring subsequent MTS chemistry. Our interest in increasing the traction of MTS for producing macrocycles tailored towards a given metal ion prompted us to re-examine the synthesis of *endo*-HXA monomers. In this work, we describe an expedited synthesis of *endo*-HXA monomers that gives significantly greater yields of product and uses a class of starting reagent that allows an expansion in structural diversity. The library of new *endo*-HXA monomers described here has been used in an MTS approach to generate a set of structurally diverse dimeric hydroxamic acid macrocycles, which have been characterized as holo-(Fe(III)-loaded) complexes and apo-(Fe(III)-free) ligands. These results provide the potential to expand MTS to generate new macrocycles with structures that deviate beyond those of natural products.

Results and discussion

Synthesis of *endo*-hydroxamic acid amino carboxylic acid (*endo*-HXA) monomers

The first described synthesis of PBH undertook a reaction between *O*-benzyl-*N*-(4-cyanobutyl)hydroxylamine and succinic anhydride followed by nitrile-to-amine reduction (Raney Ni), and *O*-benzyl deprotection (H_2 over Pd/C).[36,38,39] The reaction conditions were harsh, and furnished PBH in an overall yield of 17% (Scheme 1a). A subsequent synthetic scheme used milder conditions[37] and has been widely adopted by others,[29,31,32,40] although the route is time intensive and low yielding (Scheme 1b).

The current work began by considering improvements to the synthetic efficiency of *endo*-HXA monomers. Modifications aimed to improve the synthetic route at the level of yield, reaction times and/or safety, and are discussed with reference to PBH. First, the more

commonly used starting reagent in the more recent method (Scheme 1b) 1,5-dibromopentane or 1-bromo-5-chloropentane was replaced with 1-amino-5-pentanol (Scheme 2). The initial stage of the installation of the hydroxamic acid group involved the reaction between *N*-Boc-1-amino-5-pentanol and either *O*-*tert*-butyl-*N*-(2-nitrophenylsulfonyl)hydroxylamine or *O*-benzyl-*N*-(2-nitrophenylsulfonyl)hydroxylamine under Mitsunobu conditions. The *N*,*O*-bis-protected hydroxylamine reagents have been prepared in previous work[41] and used in the synthesis of hydroxamic acid-based compounds, including DFOB.[42] The NH group in these reagents is sufficiently acidic (pK_a 5.1) for use in the Mitsunobu reaction. The 2-nitrophenylsulfonyl (nosyl) *N*-protecting group was selected since it could be removed under mild conditions with a thiolate in an orthogonal fashion to the *O*-(*tert*-butyl)-*N*-alkyl-hydroxylamine (Scheme 2, PG_1) and the *O*-benzyl-*N*-alkyl-hydroxylamine (Scheme 2, PG_2) protecting group systems. The nosyl protecting group has been used in the synthesis of linear hydroxamic acids and to prepare other type of ligands for radiochemistry.[41-43] Following the reaction with succinic anhydride to complete the installation of the hydroxamic acid group, PBH could be generated from the *O*-*tert*-butyl-protected intermediate upon global deprotection with trifluoroacetic acid (TFA), or from the *O*-benzyl-protected intermediate with removal of the *N*-Boc group with dilute TFA followed by hydrogenation over Pd/C. The intermediates were readily purified using auto flash chromatography with the purity increasing from **13**–**16** (80%) to **17**–**22** (95%) to **1**–**6** (95%). The purity of **1**–**6** was sufficient to proceed to MTS without the need for resource and/or time-intensive preparative HPLC.

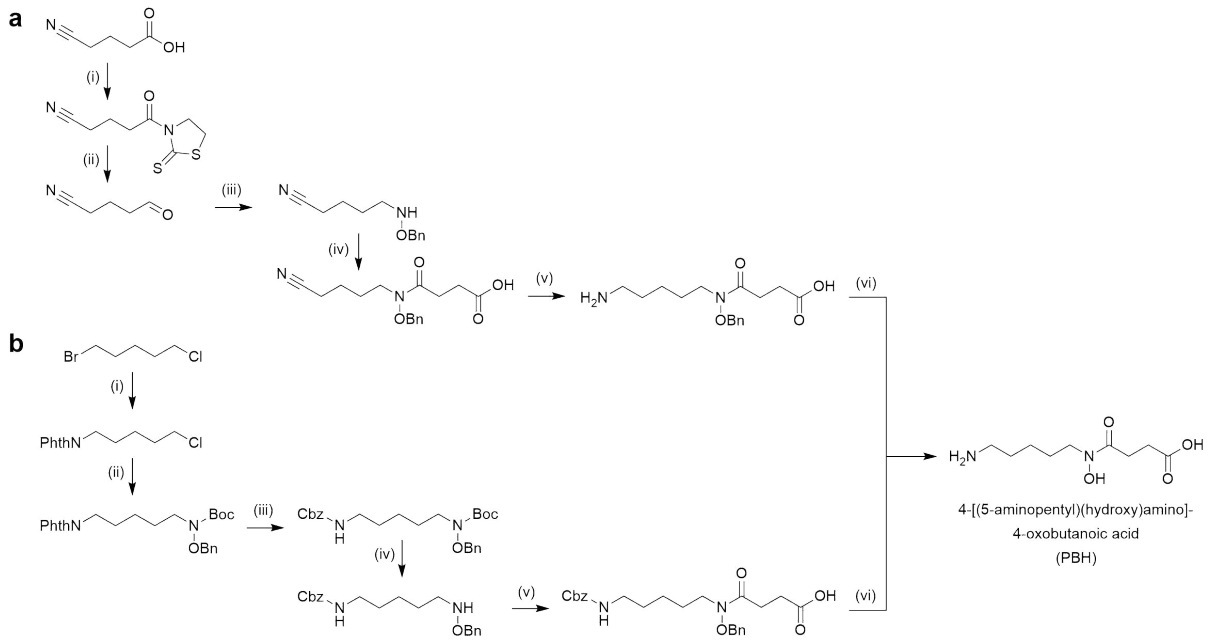

Scheme 1. Previous syntheses of the archetypal *endo*-HXA 4-[(5-aminopentyl)(hydroxy)amino]-4-oxobutanoic acid (PBH) *via* route (**a**)[36,38,39] or (**b**).[37] Conditions (**a**): (**i**) thiazolidine-2-thione, CH_2Cl_2, Et_3N, 2-chloro-1-methylpyridinium iodide, r.t., 24 h, yield not specified (**ii**) diisobutylaluminium hydride, toluene, –78 °C, 2 h, then –40 °C, 3 h, 61%, (**iii**) BnO-NH_3Cl, H_2O, MeOH, KOH, 1 h, 0 °C, then $NaBH_3CN$, HCl in MeOH, 3 h, 84%, (**iv**) succinic anhydride, pyridine, 100 °C for 1.5 h, then r.t. overnight, 98%; (**v**) H_2/Raney Ni/NH_3/CH_3OH, 0 °C, 3 h, 90%, (**vi**) H_2, 10% Pd/C, CH_3OH, HCl, 3 h, 23%; (**b**): (**i**) potassium phthalimide, DMF, 20 h, 84%, (**ii**) BnO-NH-Boc, NaH, NaI, DMF, 19 h, 85 °C, 82%, (**iii**) NH_2NH_2, EtOH, 3 h, 90 °C; CbzCl, H_2O, 1,4-dioxane, 0–20 °C, 12 h, 85% (2 steps) (**iv**) 20% TFA, 2 h, 20 °C, 76%, (**v**) succinic anhydride, pyridine, 100 °C, 2 h, then 20 °C for 12 h, 72%, (**vi**) H_2, 10% Pd/C, ^{t}BuOH, 1,4-dioxane, HCl, 3 h, 100%.

The new synthetic path developed here provided an improvement in overall yield and time-efficiency, compared to earlier methods. The overall yield (Scheme 2) was 49% and the overall reaction time for 5 (PG_1) or 6 (PG_2) steps was about 24 h. This compared to an overall yield of 10% and 65 h (6 steps) for the earliest devised synthesis (Scheme 1a),[36,38,39] or 32%

and 75 h (7 steps) for the more recent synthesis (Scheme 1b).[37] In addition to gains in synthetic efficiency, the new route allowed for expanded structural diversity, due to the availability of different types of amino-alcohol start reagents and gave more flexibility, due to the orthogonality of the *N*-protecting groups.

This work focused on PPH as the primary *endo*-HXA monomer, which has been used successfully in previous MTS approaches. PPH contains an additional methylene group in the dicarboxylic acid-containing region than PBH and is prepared by replacing succinic anhydride with glutaric anhydride (PPH, **1**). The replacement of 1-amino-5-pentanol with 2-(2-aminoethoxy)ethanol gave a PPH analogue with an ether oxygen atom in the diamine-containing region (PPH^{N}O, **2**). A thioether atom could be introduced in the diamine-containing region using 2-((2-aminoethyl)thio)ethanol as the start reagent, although this was not pursued here, to maintain a reasonable scope of workload. The replacement of glutaric anhydride with 1,4-dioxane-2,6-dione or 1,4-oxathiane-2,6-dione, gave PPH analogues containing an ether (PPH^{C}O, **3**) or thioether (PPH^{C}S, **5**) atom in the dicarboxylic acid-containing region. Replacements in both the diamine- and the dicarboxylic acid-containing regions gave *endo*-HXA ligands containing variable substitutions of ether and thioether groups (PPH^{N}O^{C}O, **4**; PPH^{N}O^{C}S, **6**) (Scheme 2).

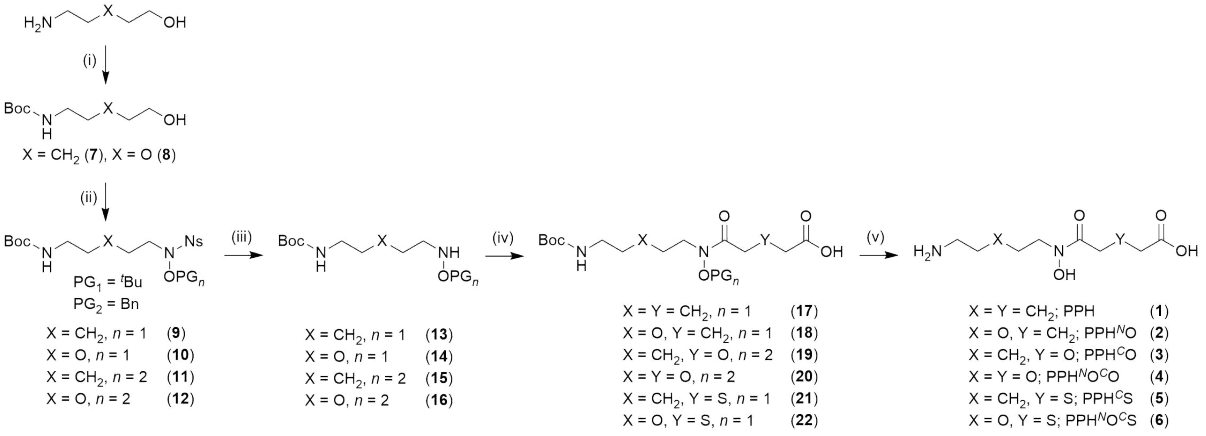

Scheme 2. Improved synthesis of *endo*-HXA monomers **1**–**6**. Conditions: (**i**) Boc_2O, Et_3N, DCM, r.t., 4 h, (**ii**) ^{t}BuO-NH-Ns (*n* = 1) or BnO-NH-Ns (*n* = 2), Ph_3P, DIAD, THF, 40 °C, 8 h, (**iii**) 2-mercaptoethanol, DBU, DMF, r.t., 3 h, (**iv**) glutaric anhydride (**1**, **2**), 1,4-dioxane-2,6-dione (**3**, **4**), or 1,4-oxathiane-2,6-dione (**5**, **6**), DCM, r.t., 3 h (**v**) TFA:DCM 9:1, r.t., 4 h (*n* = 1), or TFA:DCM 1:9, r.t., 2 h; H_2, 10% Pd/C, ^{t}BuOH, 60 °C, 0.5 h (two steps) (*n* = 2). PG_1 was used for **1**, **2**, **5** and **6**. PG_2 was used for **3** and **4**.

A further improvement was gained in the reaction step with the anhydride (Scheme 2, step (iv)) by replacing pyridine with dichloromethane and triethylamine. The triethylamine base was subsequently determined to be unnecessary. These modifications mitigated the high variability in yields (40–80%) and reduced the reaction time for this step from 24 h to 3 h. Use of the *O*-*tert*-butyl protecting group for the hydroxamic acid was first pursued as a general method for *endo*-HXA ligands, since this could potentially enable global deprotection of the N–*O*^{t}Bu group and the NH–Boc group with high concentrations of TFA. However, similar to observation from others,[42] in some instances the high concentration of TFA promoted the hydrolysis of the hydroxamic acid group. This reactivity was dependent upon the nature of the anhydride employed in the reaction. The N–*O*^{t}Bu protecting group strategy was incompatible with 1,4-dioxane-2,6-dione, but was compatible with glutaric anhydride and 1,4-oxathiane-2,6-dione. This was fortuitous in the case of 1,4-oxathiane-2,6-dione, since this mitigated issues with sulfur poisoning the catalyst in the Pd/C reductive deprotection route. The 1,4-dioxane-2,6-dione system required the use of a N–*O*Bn protecting group, necessitating a two-step deprotection procedure (Scheme 2, step (v)). The instability of ether-containing molecules towards N–*O*^{t}Bu deprotection has been reported.[42] All *endo*-HXA ligands **1**–**6** were characterised using ^{1}H and ^{13}C and ^{1}H-^{1}H COSY NMR spectroscopy and HRMS (Fig. S1–S6).

Synthesis of Fe(III)-loaded dimeric hydroxamic acid macrocycles 1a–6a using MTS

The set of *endo*-HXA monomers **1**–**6** allowed an examination of the synthesis of new hydroxamic acid macrocycles using MTS. MTS relies on the formation of a metal-ligand supramolecular assembly in which the terminal amine and carboxylic acid groups of contiguous *endo*-hydroxamic acid amino carboxylic acid monomers are suitably positioned to allow ring closure upon *in situ* peptide coupling. This is designed to provide facile access to metal-loaded macrocycles (holo-macrocycles), with apo-macrocycles accessible upon incubation with a high concentration of chelator to compete for the templating metal ion (Scheme 3). The MTS reaction was conducted using a 1:2 Fe(III):ligand stoichiometry, with *in situ* amide-bond forming chemistry undertaken with DPPA and triethylamine.

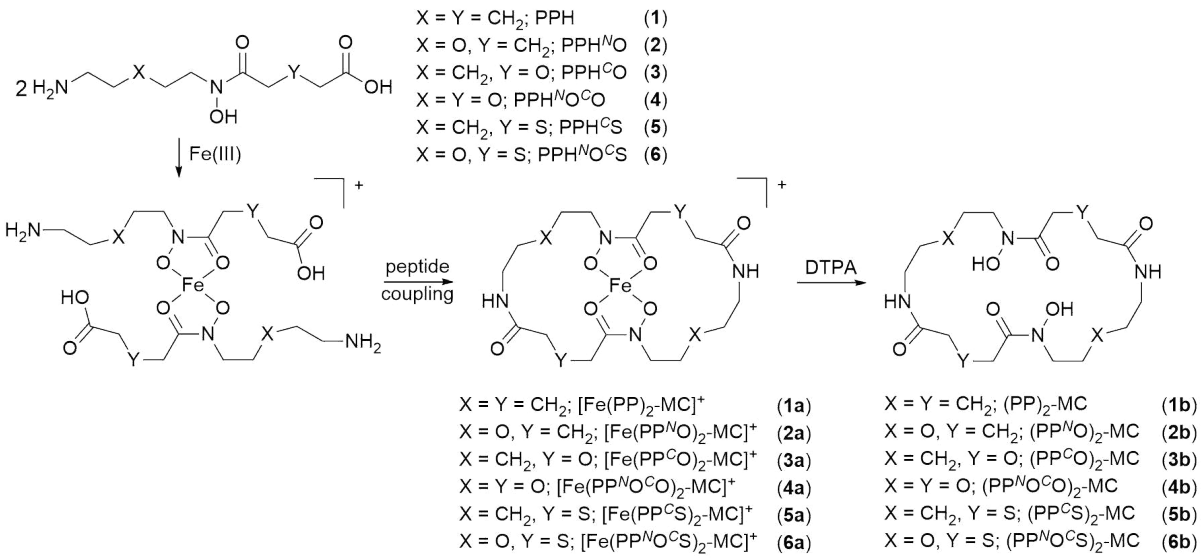

Scheme 3. Synthesis of dimeric hydroxamic acid macrocycles as Fe(III) complexes (holo-macrocycles: **1a**–**6a**) or as free ligands (apo-macrocycles: **1b**–**6b**).

The MTS reaction solution was analysed using LC-MS, with selected ion monitoring (SIM) as the detection mode. The 1:2 Fe(III):ligand stoichiometry was selected to promote the

generation of dimeric macrocycles (Table 1). It was possible that the MTS system might generate trimeric macrocycles, since this configuration would stabilise the octahedral coordination preference of Fe(III). The SIM values selected for the analysis correlated with the intrinsically charged Fe(III)-dimeric macrocycle ($[M]^+$) and the protonated adduct ($[M+H]^+$) of the neutral Fe(III)-trimeric macrocycle.

Table 1 HPLC retention times for holo-macrocycles **1a**–**6a** and apo-macrocycles **1b**–**6b**

Holo-macrocycle		t_R (min)	m/z_{exp}	Apo-macrocycle		t_R (min)	m/z_{exp}	*c*log*P*[a]	*c*log*P*[b]
$[Fe(PP)_2\text{-}MC]^+$	**1a**	21.0	482.2	$(PP)_2\text{-}MC$	**1b**	27.6	429.1	–2.84	0.64
$[Fe(PP^NO)_2\text{-}MC]^+$	**2a**	20.9	486.2	$(PP^NO)_2\text{-}MC$	**2b**	21.4	433.4	–5.93	–0.71
$[Fe(PP^CO)_2\text{-}MC]^+$	**3a**	25.8	486.2	$(PP^CO)_2\text{-}MC$	**3b**	29.7	433.3	–5.12	–1.48
$[Fe(PP^NO^CO)_2\text{-}MC]^+$	**4a**	21.4	490.2	$(PP^NO^CO)_2\text{-}MC$	**4b**	17.9	437.2	–8.21	–3.61
$[Fe(PP^CS)_2\text{-}MC]^+$	**5a**	30.4	518.2	$(PP^CS)_2\text{-}MC$	**5b**	30.2	465.2	–3.47	–0.40
$[Fe(PP^NO^CS)_2\text{-}MC]^+$	**6a**	22.4	522.1	$(PP^NO^CS)_2\text{-}MC$	**6b**	22.9	469.3	–6.56	–2.53

[a] Calculated using ACD/ChemSketch 2017.2.1. [b] Calculated using Molinspiration (https://www.molinspiration.com/cgi-bin/properties)

Signals in the LC were detected for each of **1a**–**6a** (Figure 1, upper row). Aside from the well-resolved and narrow signal for **5a**, these signals were broad (**3a**) and commonly contained a low-intensity shoulder (**1a**, **2a**, **4a**, **6a**), which could be due to the presence of a distribution of Fe(III)-macrocycle conformers that were partially resolved by the LC conditions. The experimental MS isotope pattern at the peak maxima (Figure 1, middle row) for **1a**–**6a** correlated well with calculated isotope patterns (Figure 1, lower row). The LC signals were ascribed to the dimeric hydroxamic acid Fe(III)-macrocycles, as determined

from EIC measurements, which correlated strongly with the SIM traces (Fig. S7, top and middle rows). EIC signals that corresponded with the $[M+H]^+$ adducts of the trimeric Fe(III)-macrocycles were discernible only at baseline levels (Fig. S7, lower row), which showed the MTS reaction stoichiometry favoured the formation of the dimeric macrocycles. The signal for **5a** at *m*/*z* 518.2 was present with a signal at *m*/*z* 501.1 ascribable to co-eluting diphenyl hydrogen phosphate $[2M+H]^+$ as a product of DPPA-mediated peptide coupling.[44,45]

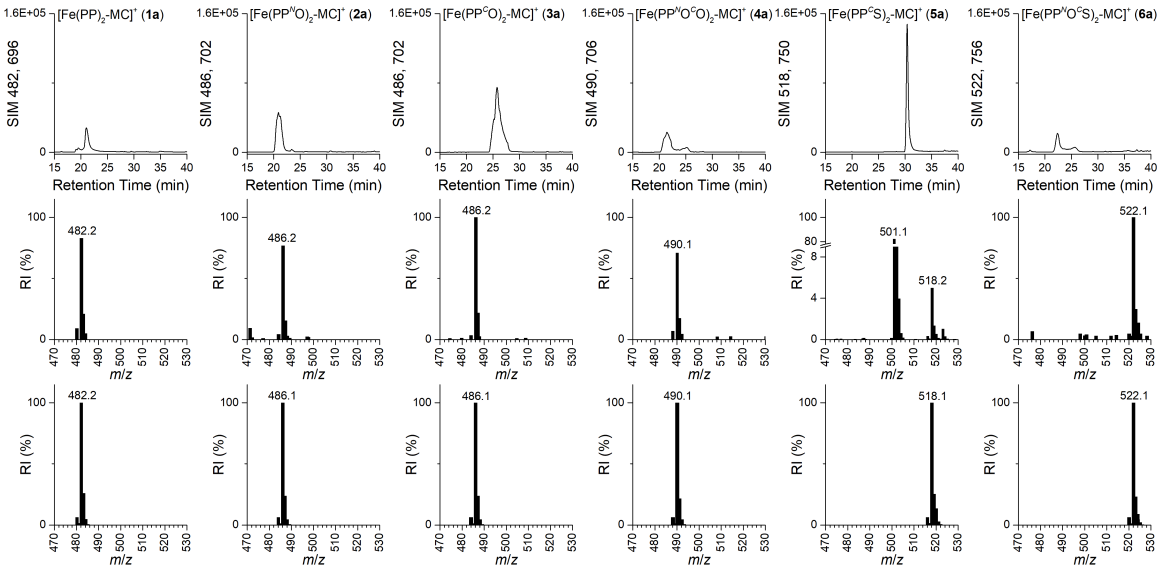

Figure 1. Complexes between Fe(III) and dimeric hydroxamic acid macrocycles (**1a**–**6a**) produced using MTS, as characterised using LC-MS (SIM detection) (upper row, left to right), with experimental (middle row) or calculated (lower row) isotope patterns shown in each corresponding column.

Production of apo-dimeric hydroxamic acid macrocycles

The Fe(III) template was removed from **1a**–**6a** using diethylenetriaminepentaacetic acid (DTPA) as a chelator proven effective for this purpose.[29] The MTS reaction solutions containing **1a**–**6a** were each treated with excess DTPA to compete for the Fe(III) template and liberate the corresponding apo-macrocycle **1b**–**6b**. LC signals for **1b**–**4b** and **6b** appeared

as sharp, single peaks (Figure 2, upper row), with experimental MS isotope patterns (Figure 2, middle row) in agreement with calculated data (Figure 2, lower row). The major MS signal correlated with the $[M+H]^+$ adduct of the neutral apo-macrocycle, with lower intensity signals present for sodium and potassium adducts. The solutions were analysed for the presence of Fe(III)-free trimeric macrocycles, with minor peaks detected at <1% area of the dimeric analogues (Fig. S8). In the case of **5b**, two well resolved signals were observed at t_R 30.2 min (peak 1) and t_R 38.5 min (peak 2). The EIC data (Fig. S8, middle row) showed that each peak was ascribable to a species with SIM 465. These two peaks were separated using semi-preparative HPLC for further analysis (Fig. S9). As expected, MS analysis of the separate solutions gave isotope patterns at 465.2 (peak 1) or 465.3 (peak 2). It was likely that one of these peaks was ascribable to **5b** and that the second peak was due to an artefact of the reaction and/or side-product. The authenticity of **5b** was confirmed upon adding an aliquot of Fe(III) to each isolated solution. In the case of peak 1, the holo-macrocycle **5a** was re-constituted (Fig. S9e, g), while no LC signal was observed for **5a** from a solution of Fe(III) and peak 2 (Fig. S9f). This identified peak 1 as apo-macrocycle **5b** and peak 2 as a species that had an *m*/*z* value coincident with **5b** but that was not relevant as a target. The species in peak 2 was present in the MTS mixture containing **5a**, as detected by EIC at 465 (Fig. S9a, grey).

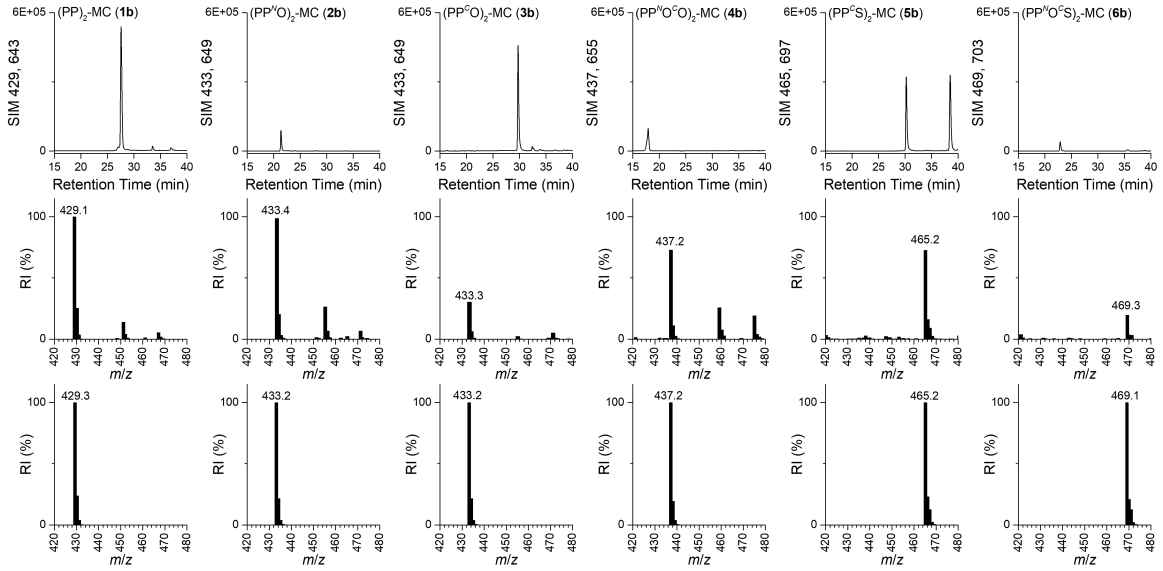

Figure 2. Dimeric hydroxamic acid apo-macrocycles (**1b**–**6b**) detected upon removing Fe(III) from **1a**–**6a**, as characterised using LC-MS (SIM detection) (upper row, left to right), with experimental (middle row) or calculated (lower row) isotope patterns shown in each corresponding column.

A more accurate comparison of LC retention times for **1b**–**6b** was obtained from acquiring the LC trace from a mixture of the apo-macrocycles that had been isolated as individual fractions from the LC, with the authenticity of each compound shown using HRMS (Fig. S10–S15). The LC trace from this composite solution (Figure 3a) showed a positive correlation between the *c*Log*P* values and the LC retention time for **1b**–**6b** (r = 0.82 or 0.62 for ACD ChemSketch or Molinspiration *c*LogP calculators, respectively) (Figure 3b). The data points for **2b** and **3b** were the most significant outliers from the line of best fit. Despite the presence of two ether oxygen atoms, which would be expected to increase polarity, **3b** eluted in a less polar window than the methylene isostere **1b**. Apo-macrocycle **4b**, which contained four ether oxygens, eluted in the most polar region of the LC. Apo-macrocycle **2b** eluted in the second most polar region of the LC and in a significantly different window to the isomer **3b**. This showed the position of the ether oxygen atom in the

diamine-containing region (**2b**) or the dicarboxylic acid-containing region (**3b**) had a significant effect on the solvation properties, based on the surrogate measure of LC retention time.

The retention time of the holo-macrocycles **1a**–**6a** (Figure 2) and the corresponding apo-macrocycles **1b**–**6b** (Figure 1) were examined (Figure 3c). In the case of the systems **2**, **5** and **6**, the retention time of the holo- and apo-macrocycles were similar. In the case of systems **1** and **3**, the removal of Fe(III) produced a free ligand that eluted in a less polar LC window than the Fe(III) complex. System **4** showed the opposite trend, with the apo-macrocycle eluting in more polar LC window than the Fe(III) complex. These qualitative observations demonstrate the effects of the type of group present in a macrocycle (methylene, oxygen, sulfur), its position, and the presence or absence of Fe(III) on the LC elution behaviour as a proxy of solvation properties. This demonstrates the potential of introducing elements of structural diversity into a siderophore macrocycle to moderate its properties.[46,47]

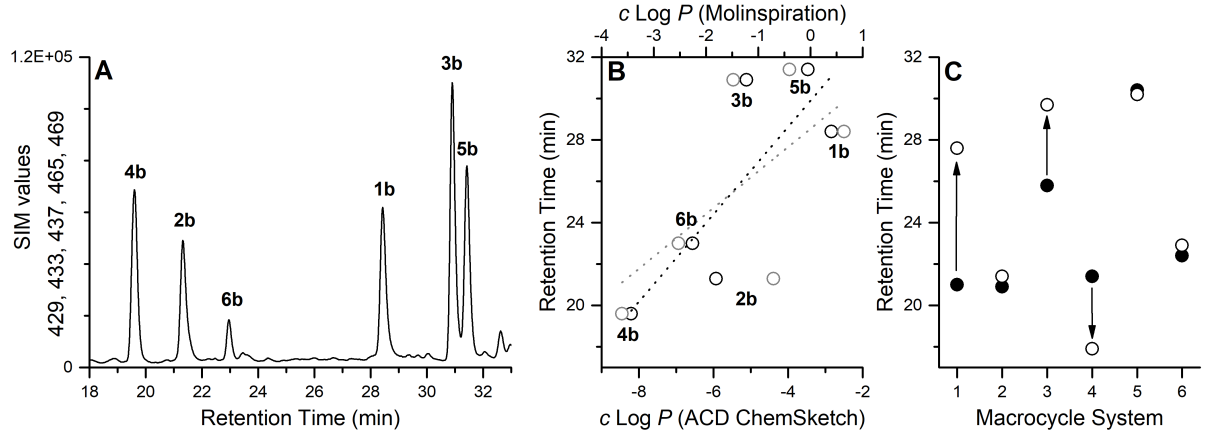

Figure 3. LC from a mixture of isolated solutions of **1b**–**6b** with detection using multiple SIM values (A), a plot of *c*Log*P* values of **1b**–**6b** versus retention time (B) using ACD ChemSketch (black) or Molinspiration (grey) calculators, and a plot of the retention time of the apo-macrocycles **1b**–**6b** (open circles) and the corresponding holo-macrocycles **1a**–**6a** (closed circles) (C, using data from Figure 1 and Figure 2).

Density functional theory (DFT) calculations of 1b–6b

Density functional theory (DFT) calculations were used to calculate selected molecular properties and estimate the solvation energetics of **1b–6b** (Table 2). Of most interest was to provide a rationale for the significant difference in RP-HPLC retention times observed by experiment for the constitutional isomers **2b** and **3b**. Although no symmetry constraints were imposed, all of the structures of **1b–6b** converged with pseudo-C_2 symmetry with the rotation axis positioned through the cavity of the macrocycle (Figure 4, Table S1–S6).

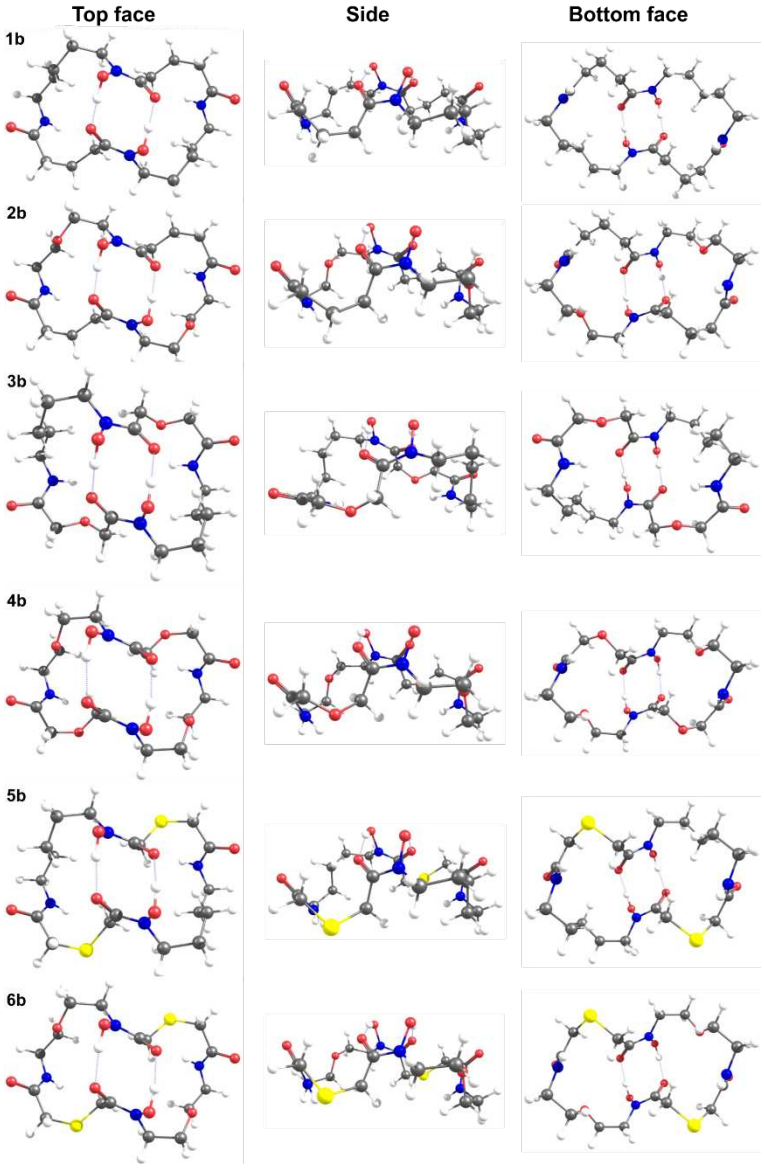

Figure 4. Three projections of the optimised structures of **1b**–**6b** calculated using the B3LYP/DGDZVP/PCM methodology.

Analysis of the calculated molecular properties for **1b**–**6b** indicated **3b** as an outlier, particularly in terms of the calculated dipole moment. The calculated dipole moments (μ) of **1b**, **2b** and **4b**–**6b** ranged between 13.0 to 17.7 D (Table 2), with the value for **3b** (μ = 3.7 D) showing a reduced polarity. Origins of this difference lie in the steric and electronic constraints imposed by inserting the ether group between the two carbonyl groups. In this position, the ether oxygen atom forces the amide groups to twist and point away from the macrocyclic cavity (essentially orthogonal to the pseudo-C_2 axis). In contrast to the other compounds in the series, this twist in **3b**, reduces the polarity and the dipole moment. The effect can be seen in the electrostatic potential maps of **2b** and **3b** (Figure 5). No such difference was observed in the calculated properties or optimised structure of **5b**, which contains a thioether group in place of the ether group of **3b** (Figure S16). The larger sulfur atom in **5b** allows for increased conformational flexibility in the ring. Placing the ether group in the centre of the diaminopentane-derived region in **2b** did not induce the same conformational restrictions, with **2b** retaining a high polarity. No discernible trend was observed in the calculated solvation energies (Table 2).

Table 2 Summary of the calculated molecular properties and solvation energetics of **1b**–**6b**

Apo-macrocycle		Dipole mom	Polarisability, μ (a.u.)	Cavity volume (Å^3)	Cavity surface area (Å^2)	Electronic spatial extent	ΔH_{solv} (kJ mol^{-1})	ΔS_{solv} (J K^{-1} mol^{-1})	ΔG_{solv} (kJ mol^{-1})

		ent, μ (D)				<R^2> (a.u.)			
$(PP)_2$-MC	**1b**	14.4	349	604	494	13103	–41.7	–41.7	–41.1
$(PP^NO)_2$-MC	**2b**	17.7	326	587	495	13070	–40.8	–36.6	–40.5
$(PP^CO)_2$-MC	**3b**	3.7	329	582	482	13040	–83.1	–83.7	–83.0
$(PP^NO^CO)_2$-MC	**4b**	15.2	305	561	465	12566	–62.1	–64.6	–61.1
$(PP^CS)_2$-MC	**5b**	13.0	374	613	496	14509	–87.1	–87.5	–86.9
$(PP^NO^CS)_2$-MC	**6b**	15.8	352	595	497	14340	–58.2	–59.8	–57.0

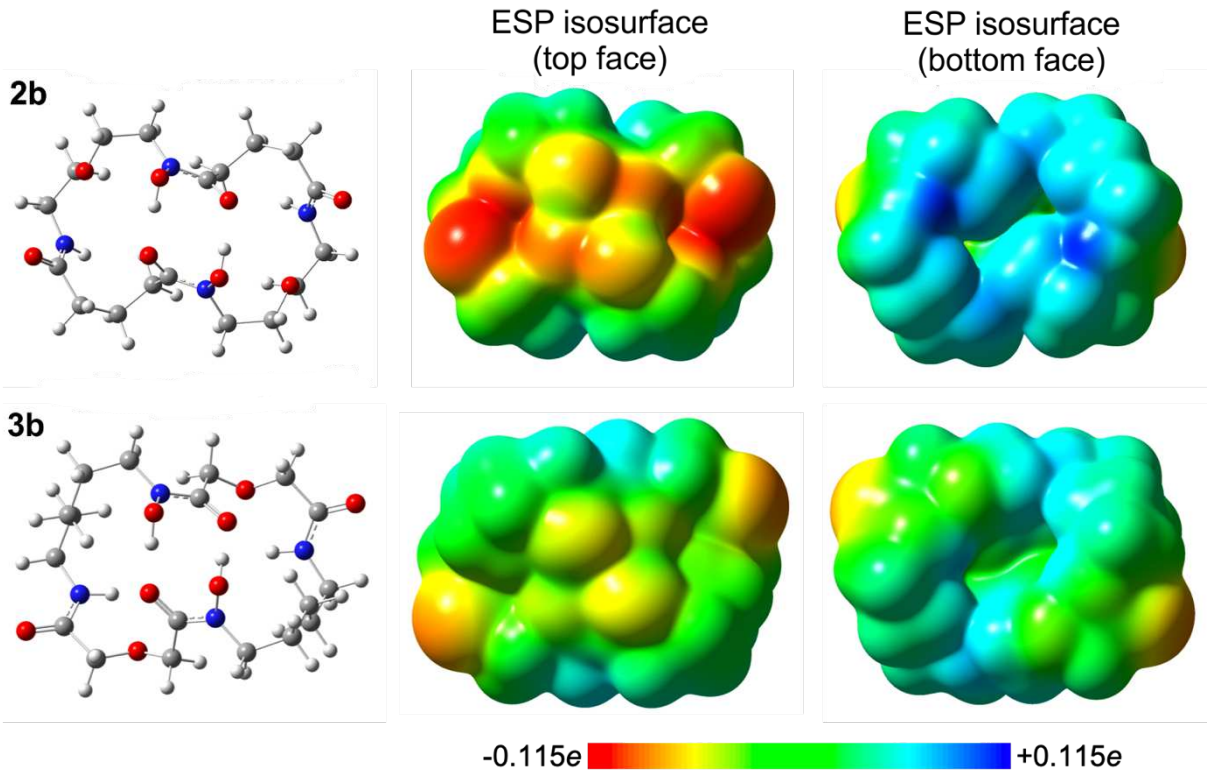

Figure 5. DFT optimised structures of **2b** and **3b**, and the calculated electrostatic potential maps (ESP; with charge in the range –0.115*e* to 0.115*e*) showing projections from the top face (centre) as viewed down the pseudo-C_2 rotation axis, and the opposing bottom face (right). ESPs are projected onto the total electron density isosurface (at the 99.9% cut-off).

Structures were optimised using the B3LYP/DGDZVP methodology and calculations included solvation effects in water using a polarisable continuum model (PCM).

Conclusion

This work has reported a new synthesis for *endo*-HXA monomers that furnishes these ligands in higher yields (2–5 times greater) and in less time (3–4 times less) than previous methods. The use of the nosyl protecting group adds value to the synthesis through its orthogonality to other *N*-protecting groups and its removal under mild conditions. The amino-alcohol reagent used in the first step allows an expansion in structural diversity in *endo*-HXA monomers, due to the ready availability of different analogues. The *endo*-HXA ligands **1**–**6** were used in successful MTS reactions in a 1:2 Fe(III):ligand stoichiometry to produce the corresponding Fe(III)-loaded dimeric hydroxamic acid macrocycles **1a**–**6a**, which following treatment with DTPA, gave the apo-macrocycles **1b**–**6b**. Apo-macrocycles **1b**–**6b** gave different retention times on an RP-HPLC column, which reflected different solvation properties ascribable to the presence and position of methylene groups and ether and/or thioether atoms. The optimised structures and solvation properties of the ether-containing isomers **2b** and **3b** were examined by DFT calculations. Results confirmed that **3b** was anomalous in the series and that an ether group positioned between the carbonyl centres imposed steric and electronic constraints that invoked a twist in the macrocycle which reduced the molecular polarity. Improved access to *endo*-HXA monomers could support MTS as a more robust method for generating metal-tailored macrocycles and other syntheses requiring these types of ligands. The increased yields of *endo*-HXA ligands will better support our current efforts in obtaining X-ray crystal structures of the MTS-generated macrocycles.

Experimental procedures

All reactions were performed under an inert nitrogen atmosphere. The progress of reactions was monitored by thin layer chromatography (TLC), with plates visualized using UV light at 254 nm or by staining with ninhydrin, vanillin or $FeCl_3$. ^1H and ^{13}C nuclear magnetic resonance (NMR) spectroscopy was performed on a Bruker 600 MHz AVIIII with a TCI cryoprobe at 25 °C operating with Topspin 3.5 NMR software. Samples were made to a concentration of 10 mg mL^{-1} in $CDCl_3$ (Sigma-Aldrich, 99.8%), CD_3OD (Cambridge Isotope Laboratory, 99.8%) or DMSO-d_6 (Cambridge Isotope Laboratory, 99.9%). Chemical shifts are reported in ppm relative to the residual solvent peaks ($CDCl_3$: δ_H 7.27 ppm, δ_C 77.23 ppm; CD_3OD: δ_H 3.31 ppm, δ_C 49.00 ppm; DMSO-d_6: δ_H 2.50 ppm, δ_C 39.52 ppm). Signal multiplicities are labelled as: s (singlet), d (doublet), t (triplet), q (quartet), qn (quintet) or m (multiplet). Coupling constants are designated *J* (Hz). High-resolution mass spectrometry (HRMS) was conducted on a Bruker solariX 2XR 7T Fourier Transform Ion Cyclotron Mass Spectrometer in the School of Chemistry, University of Sydney.

General Procedures

Reagents

1-Amino-5-pentanol (95%), 2-(2-aminoethoxy)ethanol (98%), 1,8-diazabicyclo[5.4.0]undec-7-ene (DBU, 98%), dichloromethane (≥ 99.8%), 1,4-dioxane-2,6-dione (common name: diglycolic anhydride, 95%), diisopropyl azodicarboxylate (DIAD, 99%), diphenylphosphoryl azide (DPPA, 97%), di-*tert*-butyl dicarbonate (99%), glutaric anhydride (95%), iron(III) acetylacetonate (97%), triethylamine (≥ 99%), methanol (99.8%), 2-mercaptoethanol (≥ 99%), *N,N*-dimethylformamide (99.8%), succinic anhydride (≥ 99%), tetrahydrofuran (≥ 99%), *tert*-butanol (≥ 99.5%) and trifluoroacetic acid (99%) were purchased from Sigma-Aldrich (Castle Hill, Australia). Hexane and ethyl acetate were purchased from Thermofisher Scientific (Sydney, Australia). 1,4-Oxathiane-2,6-dione (thiodiacetic anhydride) (98%) was

purchased from Fluorochem (Hadfield, United Kingdom). All solvents were anhydrous unless stated otherwise. All chemicals were used as received. Milli-Q water was used for all experiments, as required.

Instrumentation

Silica chromatography

Flash chromatography was performed on a Grace Reveleris X2 Auto Flash system using hexane and ethyl acetate as solvents, unless specified otherwise. The cartridges sizes and flow rates were varied depending on the scale of the reaction: 0.1–1 g-scale reaction (cartridge = 12 g, flow rate = 30 mL min^{-1}), 1–8 g-scale reaction (cartridge: 40 g, flow rate = 40 mL min^{-1}). Methods were developed using the Reveleris auto-gradient feature based on R_f values from TLC experiments. Crude compounds were dissolved in a minimum amount of ethyl acetate and injected onto the column *via* the injection port.

Reverse-phase liquid chromatography-mass spectrometry

Reverse-phase liquid chromatography-mass spectrometry (RP LC-MS) was employed using an Agilent Technologies HPLC system (Santa Clara, CA) consisting of an autoinjector (100 μL loop), an Agilent 1260 Infinity degasser, a quaternary pump and an Agilent 6120 Series Quadrupole electrospray ionization (ESI) mass spectrometer. An Agilent C18 column reverse-phased prepacked column (4.6 × 150 mm i.d., particle size 5 μm) was used for all experiments. Agilent OpenLAB Chromatography Data System (CDS) ChemStation Edition was used to process mass chromatograms in each of the scan and the selected ion monitoring (SIM) or extraction ion chromatogram (EIC) detection modes. Samples were made to a concentration of 1 mg mL^{-1} in MeOH or for MTS samples in 1:1 DMF:H_2O. The following

instrumental conditions were used: flow rate 0.5 mL min^{-1}, injection volume 5 µL, spray voltage 4 kV, capillary voltage 3 kV, capillary temperature 250 °C, tube lens offset 10 V. Mobile phases were prepared by mixing acetonitrile (ACN):formic acid (99.9:0.1, mobile phase B) and H_2O:formic acid (99.9:0.1, mobile phase A). Method A: 0–100% ACN:H_2O gradient over 45 min. Method B: 0–28% ACN:H_2O gradient over 40 min.

H-Cube

Hydrogenation was performed on an H-cube Mini Plus with a micro HPLC pump. The 10% Pd/C CatCart was from ThalesNano (ID: THS-01111). The mobile phase was prepared by mixing *tert*-butanol:ethyl acetate (9:1). The method used a temperature of 60 °C and a flow rate = 1 mL min^{-1} with a run time = 20 min.

General Methods

Metal-templated synthesis

A methanol solution (1 mL) containing **1** (4.1 mg, 17.6 µmol) was added to a methanol solution (1 mL) containing $Fe(acac)_3$ (3.1 mg, 8.8 µmol) to give a 2 mg mL^{-1} solution with respect to **1**. The solution was stirred for 2 h and the solvent was removed *in vacuo* and the product was dried under high vacuum overnight. DMF (4 mL) was added to the crude mixture followed by the addition of DPPA (29 µL, 35.2 µmol) and Et_3N (10.7 µL, 35.2 µmol). The reaction mixture was stirred for 5 d and aliquots of 100 µL were taken from the mixture and diluted with milli-Q water (100 µL) to quench the reaction. Analogous procedures were conducted for **2**–**6**. Reaction mixtures were analysed by LC-MS (positive ion) using TIC, SIM and EIC detection modes.

Removing Fe(III) from holo-macrocycles 1a–6a

An aliquot of the reaction mixture (100 μL) was taken and diluted with an equivalent aliquot of DTPA (0.2 M) and the mixture was left to incubate overnight. A sample was taken and analysed by LC-MS.

Isolation of apo-macrocycles 1b–6b by HPLC

The MTS solutions treated with DTPA containing **1b**–**6b** were analysed by HRMS and were purified by HPLC (Method B). Fractions were collected over the following elution times: **1b** (26–30 min), **2b** (19–23 min), **3b** (27–31 min), **4b** (15–19 min), **5b** (peak 1, 28–32 min; peak 2, 36–40 min), **6b** (20–24 min). The ACN was removed *via* rotary evaporation and the fractions were then lyophilised to dryness. The solid was re-dissolved in 200 μL water and the solutions were pooled and analysed by LC-MS and HRMS.

Computational details

All calculations were conducted using density functional theory (DFT) as implemented in the Gaussian16 Revision A.03 suite of *ab initio* quantum chemistry programs. Normal self-consistent field (SCF) and geometry convergence criteria were employed throughout and structures were optimised without using symmetry constraints. All structures were optimised in the gas phase, and in solution phase using a polarisable continuum model (PCM) and the B3LYP/DGDZVP methodology. Solvated phase calculations were implemented by using the SCRF keyword with default parameters and selecting water as the solvent (dielectric constant, $\varepsilon = 78.3553$). Harmonic frequency analysis based on analytical second derivative was used to characterise optimised structures as local minima. The choice of solvation model reflects our standard aqueous phase conditions employed in the potential use and application of the macrocyclic chelates described in this work. Optimised structures were analysed by

using Chemcraft (version 1.8, build 536b) and GaussView 6.0.16 (Gaussian Inc., Wallingford, MA). Electrostatic potentials (calculated in the range -0.115*e* to +0.115*e*) were mapped onto the total electron density surface (set to a cut-off of 99.9% density).

Synthesis

O-Benzyl-*N*-(2-nitrophenylsulfonyl)hydroxylamine

O-Benzylhydroxylamine hydrochloride (5.0 g, 31.3 mmol) was dissolved in anhydrous pyridine (60 mL), stirred vigorously and cooled to −5 °C. A solution of 2-nitrobenzylsulfonyl chloride (7.1 g, 32.0 mmol) in pyridine (20 mL) was added dropwise. The solution was left to stir at −5 °C for 30 min then allowed to warm to r.t. and stirred for a further 2 h. H_2O (15 mL) was added to terminate the reaction and the solvents were removed *in vacuo*. The residue was re-dissolved in EtOAc:H_2O (1:1, 400 mL) and partitioned in a separatory funnel. The organic layer was washed with 5% HCl, H_2O and $NaHCO_3$ (200 mL each). The organic layer was concentrated *in vacuo* to yield the semi-pure product as an orange crystalline solid (6.9 g, 70%). **^{1}H NMR** (600 MHz, $CDCl_3$): δ_H 8.24–8.26 (m, 1H), 8.12 (s, 1H), 7.78–7.88 (m, 3H), 7.37 (s, 5H), 5.10 (s, 2H). **^{13}C NMR** (150 MHz, $CDCl_3$): δ_C 149.1, 135.6, 135.3, 132.5, 130.3, 129.7, 128.5, 124.6, 78.7. **LRMS** (ESI+): *m/z* ($[M+H]^+$, 100%): 309.2. The data are consistent with literature.[41]

O-tert-Butyl-*N*-(2-nitrophenylsulfonyl)hydroxylamine

O-tert-Butylhydroxylamine hydrochloride (5.06 g, 40.2 mmol) was dissolved in anhydrous $CHCl_3$ (80 mL) and the reaction cooled to −5 °C. Et_3N (11.7 mL, 84.4 mmol) was added dropwise, followed by the dropwise addition of a solution of 2-nitrobenzylsulfonyl chloride (8.93, 40.2 mmol) in $CHCl_3$ (50 mL). The reaction was stirred at −5 °C for 2 h, warmed to r.t.

and left stirring overnight. The reaction mixture was washed with H_2O, 1 M HCl, H_2O, 5% $NaHCO_3$, H_2O and brine (40 mL each). The organic layer was concentrated *in vacuo* to yield the product as a yellow crystalline solid (8.82 g, 80%). **^{1}H NMR** (600 MHz, $CDCl_3$): δ_H 8.15–8.16 (m, 1H), 7.78–7.86 (m, 3H), 1.26 (s, 9H). **^{13}C NMR** (150 MHz, $CDCl_3$): δ_C 148.5, 134.5, 133.8, 133.7, 132.7, 125.3, 82.9, 26.7. **LRMS** (ESI+): *m/z* ($[M+H]^+$, 100%): 275.1. The data are consistent with literature.[41]

***N*-Boc-1-amino-5-pentanol (7)**

To a solution of 1-amino-5-pentanol (1.50 g, 14.5 mmol) in CH_2Cl_2 (120 mL) was added a solution of Boc_2O (3.16 g, 14.5 mmol) in CH_2Cl_2 (10 mL). The solution was treated with Et_3N (2.22 mL, 15.9 mmol) dropwise and the mixture was stirred for 4 h. The reaction was concentrated *in vacuo* and the crude product was purified using auto flash chromatography (gradient: 30% EtOAc over 2 min, 30% to 60% over 5 min, 60% over 2 min) to afford the product as a yellow oil (90%). **^{1}H NMR** (600 MHz, $CDCl_3$): δ_H 3.67 (t, J = 6.5 Hz, 2H), 3.20 (d, J = 6.2 Hz, 2H), 1.63 (qn, J = 7.2 Hz, 2H), 1.56 (qn, J = 7.3 Hz, 2H), 1.49 (s, 9H), 1.42–1.46 (m, 2H); **^{13}C NMR** (150 MHz, $CDCl_3$): δ_C 156.1, 77.1, 62.3, 40.4, 32.2, 29.8 28.4, 22.9. **LRMS** (ESI+): *m/z* ($[M+Na]^+$, 100%): 226.1. The data are consistent with literature.[48]

***N*-Boc-2-(2-aminoethoxy)ethanol (8)**

To a solution of 2-(2-aminoethoxy)ethanol (1.52 g, 14.5 mmol) in CH_2Cl_2 (120 mL) was added a solution of Boc_2O (3.16 g, 14.5 mmol) in CH_2Cl_2 (10 mL). The solution was treated with Et_3N (2.22 mL, 15.9 mmol) dropwise and the mixture was stirred for 4 h. The reaction was concentrated *in vacuo* and the crude product was purified using auto flash chromatography (gradient: 30% EtOAc over 2 min, 30% to 60% over 5 min, 60% over 2 min), to afford the product as a yellow oil (90%). **^{1}H NMR** (600 MHz, $CDCl_3$): δ_H 5.21 (s,

1H), 3.67–3.69 (m, 2H), 3.49–3.53 (m, 4H), 3.26–3.29 (m, 2H), 1.40 (s, 9H). **^{13}C NMR** (150 MHz, $CDCl_3$): δ_C 156.3, 79.1, 72.2, 70.1, 61.2, 40.23, 28.4. **LRMS** (ESI+): *m/z* ($[M+Na]^+$, 100%): 228.1. The data are consistent with literature.[49]

***N*,*O*-Bis-protected hydroxylamine compounds 13–16**

To a solution of **7** (1.50 g, 7.38 mmol) or **8** (1.51 g, 7.38 mmol) in THF (15 mL) was added *O-tert*-butyl-*N*-(2-nitrophenylsulfonyl)hydroxylamine (2.03 g, 7.38 mmol) or *O*-benzyl-*N*-(2-nitrophenylsulfonyl)hydroxylamine (2.25 g, 7.38 mmol) and PPh_3 (5.80 g, 22.14 mmol). After stirring for 15 min, the reaction was cooled to 0 °C and DIAD (4.48 mL, 22.14 mmol) was added dropwise. The mixture was stirred for 30 min and then heated to 40 °C and stirred for 8 h. The reaction was concentrated *in vacuo,* diluted with diethyl ether, cooled to 0 °C and stirred until a precipitate formed. The mixture was filtered, and the filtrate was concentrated *in vacuo* and purified using auto flash chromatography (gradient: 9% EtOAc over 1 min, 9–28% over 10 min, 28% over 2 min) to furnish the semi-pure nosyl protected amine compound (**9**–**12**) as an orange oil. Products **9**–**12** were not further characterised and were used directly in the next step of the synthesis. The product was re-dissolved in DMF (10 mL), treated with 2-mercaptoethanol (517 µL, 7.38 mmol) and DBU (1.12 mL, 7.38 mmol) and the solution was stirred for 3 h. The reaction was concentrated *in vacuo*, diluted with water and extracted with CH_2Cl_2. The crude mixture was purified using auto flash chromatography (gradient: 10% EtOAc over 2 min, 10–25% over 4 min, 25% over 5 min), to yield **13**–**16** as a yellow oil (75% over two steps).

***tert*-Butyl (5-(tert-butoxyamino)pentyl)carbamate (13). ^{1}H NMR** (600 MHz, $CDCl_3$): δ_H 3.22 (d, J = 7.2 Hz, 2H), 2.94 (t, J = 7.1 Hz, 2H), 1.58 (qn, J = 6.2 Hz, 4H), 1.54 (s, 9H),

1.43–1.47 (m, 2H), 1.28 (s, 9H); **^{13}C NMR** (150 MHz, $CDCl_3$): δ_C 155.9, 79.0, 77.2, 52.8, 40.5, 30.0, 28.4, 27.0, 26.8, 24.5. **LRMS** (ESI+): *m/z* ($[M+H]^+$, 100%): 275.3.

***tert*-Butyl (2-(2-(*tert*-butoxyamino)ethoxy)ethyl)carbamate (14). ^{1}H NMR** (600 MHz, $CDCl_3$): δ_H 3.53 (t, J = 5.1 Hz, 4H), 3.48 (d, J = 4.6 Hz, 2H), 3.28 (s, 2H), 2.97 (t, J = 5.1, 2H), 1.55 (s, 9H), 1.29 (s, 9H). **^{13}C NMR** (150 MHz, $CDCl_3$): δ_C 156.0, 76.8, 69.8, 67.1, 60.4, 52.5, 40.3, 28.4, 26.7. **LRMS** (ESI+): *m/z* ($[M+H]^+$, 100%): 277.2.

***tert*-Butyl (5-((benzyloxy)amino)pentyl)carbamate (15). ^{1}H NMR** (600 MHz, $CDCl_3$): δ_H 7.26-7.32 (m, 5H), 4.67 (s, 2H), 3.07 (s, 2H), 2.89 (t, J = 7.1 Hz, 2H), 1.49 (qn, J = 7.5 Hz, 2H), 1.42-1.45 (m, 2H), 1.41 (s, 9H), 1.30 (qn, J = 7.7, 2H). **^{13}C NMR** (150 MHz, $CDCl_3$): δ_C 171.2, 137.9, 128.4, 128.3, 127.7, 77.4, 76.1, 51.9, 40.4, 29.9, 28.4, 27.0, 24.3. **LRMS** (ESI+): *m/z* ($[M+H]^+$, 100%): 309.2.

***tert*-Butyl (2-(2-((benzyloxy)amino)ethoxy)ethyl)carbamate (16). ^{1}H NMR** (600 MHz, $CDCl_3$): δ_H 7.26-7.33 (m, 5H), 4.69 (s, 2H), 3.58 (t, J = 5.1 Hz, 2H), 3.55 (t, J = 4.8 Hz, 2H), 3.28 (d, J = 4.6 Hz, 2H), 3.06 (t, J = 5.1 Hz, 2H), 1.42 (s, 9H). **^{13}C NMR** (150 MHz, $CDCl_3$): δ_C 156.0, 137.9, 128.4, 128.3, 127.8, 79.2, 76.0, 70.0, 67.2, 51.5, 40.4, 28.4. **LRMS** (ESI+): *m/z* ($[M+H]^+$, 100%): 311.2.

Glutarylated *N*,*O*-bis-protected hydroxylamine compounds 17–22

To a solution of **13** (401 mg, 1.46 mmol), **14** (404 mg, 1.46 mmol), **15** (450 mg, 1.46 mmol) or **16** (453 mg, 1.46 mmol) in CH_2Cl_2 (10 mL) was added either glutaric anhydride (167 mg, 1.46 mmol), 1,4-dioxane-2,6-dione (169 mg, 1.46 mmol) or 1,4-oxathiane-2,6-dione (193 mg, 1.46 mmol). The mixture was stirred for 3 h, concentrated *in vacuo* and purified using

auto flash chromatography (gradient: 29% EtOAc over 2 min, 29–61% over 7 min, 61% over 4 min) to afford the product as a white solid (**17**, **21**–**22**) or a clear oil (**18**–**20**) (85%).

5-(*tert*-Butoxy(5-((tert-butoxycarbonyl)amino)pentyl)amino)-5-oxopentanoic acid (17). **^{1}H NMR** (600 MHz, $CDCl_3$): δ_H 2.41 (qn, J = 7.4 Hz, 4H), 1.93 (qn, J = 7.0 Hz, 4H), 1.60 (t, J = 7.1 Hz, 2H), 1.46-1.47 (m, 2H), 1.41 (s, 9H), 1.27 (s, 9H), 1.23 (t, J = 7.1 Hz, 4H). **^{13}C NMR** (150 MHz, $CDCl_3$): δ_C 178.0, 171.3, 82.7, 79.2, 60.4, 40.4, 33.2, 32.9, 29.6, 28.4, 23.9, 21.0, 19.8, 19.6, 14.2. **LRMS** (ESI+): *m/z* ($[M+Na]^+$, 100%): 411.3.

11-(*tert*-butoxy)-2,2-dimethyl-4,12-dioxo-3,8-dioxa-5,11-diazahexadecan-16-oic acid (18). **^{1}H NMR** (600 MHz, $CDCl_3$): δ_H 3.75 (s, 2H), 3.56 (s, 4H), 3.34 (s, 2H), 2.50 (t, J = 7.0 Hz, 2H), 2.03 (t, J = 7.0 Hz, 2H), 1.53 (s, 9H), 1.39 (s, 9H). **^{13}C NMR** (150 MHz, $CDCl_3$): δ_C 177.9, 156.2, 79.3, 69.7, 66.2, 50.5, 40.3, 33.1, 32.1, 28.4, 27.6, 19.9. **LRMS** (ESI+): *m/z* ($[M+Na]^+$, 100%): 413.2.

11-(Benzyloxy)-2,2-dimethyl-4,12-dioxo-3,14-dioxa-5,11-diazahexadecan-16-oic acid (19). **^{1}H NMR** (600 MHz, $CDCl_3$): δ_H 7.33-7.42 (m, 5H), 4.80 (s, 2H), 4.20 (s, 2H), 4.01 (s, 2H), 3.71 (s, 2H), 3.10 (s, 2H), 1.68 (qn, , J = 7.3 Hz, 2H), 1.50 (qn, , J = 7.4 Hz, 2H), 1.43 (s, 9H), 1.32 (s, 2H). **^{13}C NMR** (150 MHz, $CDCl_3$): δ_C 172.5, 165.6, 133.7, 129.7, 129.6, 129.5, 129.0, 128.9, 76.2, 45.4, 40.3, 29.6, 28.4, 26.4, 26.2, 24.7, 22.8. **LRMS** (ESI+): *m/z* ($[M+Na]^+$, 100%): 447.2.

11-(Benzyloxy)-2,2-dimethyl-4,12-dioxo-3,8,14-trioxa-5,11-diazahexadecan-16-oic acid (20). **^{1}H NMR** (600 MHz, $CDCl_3$): δ_H 7.39- 7.45 (m, 5H), 4.91 (s, 2H), 4.31 (s, 2H), 4.20 (s, 2H), 4.10 (s, 2H), 3.66 (t, J = 5.1 Hz, 2H), 3.49 (t, J = 5.6 Hz, 2H), 3.20 (t, J = 5.5 Hz, 2H),

1.40 (s, 9H). **^{13}C NMR** (150 MHz, $CDCl_3$): δ_C 172.2, 157.0, 134.5, 129.5, 128.8, 128.4, 78.7, 76.1, 69.4, 68.1, 67.6, 66.2, 60.1, 39.9, 27.4, 24.9. **LRMS** (ESI+): *m/z* ([M+Na]$^+$, 100%): 449.2.

11-(*tert*-Butoxy)-2,2-dimethyl-4,12-dioxo-3-oxa-14-thia-5,11-diazahexadecan-16-oic acid (21). ^{1}H NMR (600 MHz, $MeOD_4$): δ_H 3.82 (s, 2H), 3.52 (s, 2H), 3.13 (t, J = 7.0 Hz, 2H), 1.56-1.59 (m, 2H), 1.53 (s, 9H), 1.44 (s, 9H), 1.37-1.41 (m, 4H). **^{13}C NMR** (150 MHz, $MeOD_4$): δ_C 172.2, 83.5, 77.9, 77.7, 77.5, 51.7, 48.8, 33.4, 33.3, 33.1, 32.9, 29.2, 27.0, 24.6. **LRMS** (ESI+): *m/z* ([M+Na]$^+$, 100%): 429.2.

11-(*tert*-Butoxy)-2,2-dimethyl-4,12-dioxo-3,8-dioxa-14-thia-5,11-diazahexadecan-16-oic acid (22). ^{1}H NMR (600 MHz, $CDCl_3$): δ_H 3.73 (s, 4H), 3.56 (s, 2H), 3.38 (s, 2H) 3.32 (s, 2H), 1.50 (s, 9H), 1.39 (s, 9H). **^{13}C NMR** (150 MHz, $CDCl_3$): δ_C 173.2, 156.5, 89.9, 79.7, 69.8, 66.0, 50.2, 49.6, 40.3, 33.9, 33.7, 28.3, 27.6. **LRMS** (ESI+): *m/z* ([M+Na]$^+$, 100%): 431.2.

***endo*-Hydroxamic acid amino carboxylic acid (*endo*-HXA) monomers 1–6**

A solution of **17** (427 mg, 1.1 mmol), **18** (429 mg, 1.1 mmol), **21** (447 mg, 1.1 mmol) or **22** (449 mg, 1.1 mmol) was prepared in CH_2Cl_2:TFA (1:9, 5 mL) and the solution was stirred for 4 h. The mixture was concentrated, re-dissolved in toluene and concentrated *in vacuo*. Water was added and the product was lyophilised yielding an orange gum. The corresponding *endo*-HXA ligand **1**, **2**, **5** or **6** was left as a TFA salt until further reaction was required (95%). A solution of **19** (467 mg, 1.1 mmol) or **20** (469 mg, 1.1 mmol) was prepared in *tert*-butanol:ethyl acetate (9:1, 18 mL) at a concentration of 50 mM and subject to hydrogenation using a H-cube Mini Plus. The collected solution was concentrated *in* vacuo and the

compound was re-dissolved in CH_2Cl_2:TFA (5 mL, 9:1) and reacted for 2 h. The mixture was concentrated and re-dissolved in toluene and concentrated *in vacuo*. Water was added and the solution was lyophilised to yield an orange gum. The corresponding *endo*-HXA ligand **3** or **4** was left as a TFA salt until further reaction was required (95%).

5-[(5-Aminopentyl)(hydroxy)amino]-5-oxopentanoic acid (PPH) (1). ^{1}H NMR (600 MHz, $MeOD_4$): δ_H 3.63 (t, *J* = 6.9 Hz, 2H, H-9), 2.92 (t, *J* = 7.2 Hz, 2H, H-6), 2.55 (t, *J* = 6.6 Hz, 2H, H-2), 2.35 (t, *J* = 7.2 Hz, 2H, H-11), 1.86-1.90 (qn, *J* = 7.0 Hz 2H, H-10), 1.68 (t, *J* = 7.0 Hz, 4H, H-3,5), 1.38-1.40 (m, 2H, H-4). **^{13}C NMR** (150 MHz, $MeOD_4$): δ_C 175.4, 173.9, 39.2, 32.5, 30.9, 26.5, 25.7, 22.9, 19.9, 19.8. **LRMS** (ESI+): *m/z* ($[M+H]^+$, 100%): 233.1. **HRMS** *m/z:* $[M+H]^+$ calcd for $C_{10}H_{21}N_2O_4$: 233.14958; found: 233.14954.

5-((2-(2-Aminoethoxy)ethyl)(hydroxy)amino)-5-oxopentanoic acid (PPH^{N}O) (2). ^{1}H NMR (600 MHz, DMSO-d_6): δ_H 7.81 (bs, 2H, NH_3·TFA, H-1) 3.69 (t, *J* = 5.9 Hz, 2H, H-6), 3.59 (t, *J* = 5.9 Hz, H-3) 3.58 (m, *J* = 5.2 Hz, H-5), 2.95 (q, *J* = 5.1 Hz, 2H, H-2), 2.40 (t, *J* = 7.2 Hz, 2H, H-11), 2.24 (t, *J* = 7.4, 2H, H-9), 1.70 (qn, *J* = 7.3 Hz, 2H, H-10). **^{13}C NMR** (150 MHz, DMSO-d_6): δ_C 174.3 (C-8), 172.9 (C-12), 66.4 (C-3, 5), 46.8 (C-6), 38.6 (C-2), 33.0 (C-9), 30.9 (C-11), 20.0 (C-10). **LRMS** (ESI+): *m/z* ($[M+H]^+$, 100%): 235.1. **HRMS**: *m/z:* $[M+H]^+$ calcd. for $C_9H_{19}N_2O_5$: 235.12885; found: 235.12867.

2-(2-((5-Aminopentyl)(hydroxy)amino)-2-oxoethoxy)acetic acid (PPH^{C}O) (3). ^{1}H NMR (600 MHz, DMSO-d_6): δ_H 7.75 (bs, 2H, NH_3·TFA, H-1), 4.32 (s, 2H, H-9), 4.10 (s, 2H, H-11), 3.47 (t, *J* = 6.8 Hz, 2H, H-6), 2.73-2.78 (m, 2H, H-2), 1.51-1.56 (m, 4H, H-3,5), 1.27 (qt, *J* = 7.4 Hz, 2H, H-4). **^{13}C NMR** (150 MHz, DMSO-d_6): δ_C 171.4 (C-8), 169.3 (C-12), 67.6 (C-9), 67.2 (C-11), 46.9 (C-6), 38.7 (C-2), 26.7 (C-3, 5), 25.6 (C-4). **LRMS**: (ESI+): *m/z*

([M+H]$^+$, 100%): 235.1. **HRMS**: *m/z:* [M+H]$^+$ calcd. for $C_9H_{19}N_2O_5$: 235.12885; found: 235.12882.

2-(2-((2-(2-Aminoethoxy)ethyl)(hydroxy)amino)-2-oxoethoxy)acetic acid (PPH^{N}O^{C}O) (4). ^{1}H NMR (600 MHz, DMSO-d_6): δ_H 7.82 (bs, 2H, NH_3·TFA, H-1), 4.08 (d, *J* = 6.4 Hz, 4 H, H-9,11), 3.66 (t, *J* = 5.4 Hz, 2H, H-6), 3.59 (t, *J* = 5.8 Hz, 2H, H-5), 3.58 (t, *J* = 5.6 Hz, 2H, H-3) *2*.95-2.96 (m, 2H, H-2). **^{13}C NMR** (150 MHz, DMSO-d_6): δ_C 171.2 (C-8), 169.9 (C-12), 67.5 (C-9), 67.2 (C-11), 66.3 (C-3), 66.0 (C-5), 46.9 (C-6), 38.6 (C-2). **LRMS** (ESI+): *m/z* ([M+H]$^+$, 100%): 237.1. **HRMS** *m/z:* [M+H]$^+$ calcd. for $C_8H_{17}N_2O_6$: 237.10811; found: 237.10803.

2-((2-((5-Aminopentyl)(hydroxy)amino)-2-oxoethyl)thio)acetic acid (PPH^{C}S) (5). ^{1}H NMR (600 MHz, DMSO-d_6): δ_H 7.69 (bs, 2H, NH_3·TFA, H-1), 3.54 (s, 2H, H-9), 3.49 (t, *J* = 6.7 Hz, 2H, H-6), 3.34 (s, 2H, H-11) (peak co-incident with water peak; analysed by HSQC) 2.75-2.76 (m, 2H, H-2), 1.53 (t, *J* = 7.1 Hz, 4H, H-3,5), 1.27 (t, *J* = 7.1 Hz, 2H, H-4). **^{13}C NMR** (150 MHz, DMSO-d6): δ_C 170.9 (C-8), 168.7 (C-12), 47.0 (C-6), 38.7 (C-2), 33.4 (C-11), 32.6 (C-9), 26.6 (C3,5), 25.6 (C-4). **LRMS** (ESI+): *m/z* ([M+H]$^+$, 100%): 251.1. **HRMS** *m/z:* [M+H]$^+$ calcd. for $C_9H_{19}N_2O_4S$: 251.10600; found: 251.10565.

2-((2-((2-(2-Aminoethoxy)ethyl)(hydroxy)amino)-2-oxoethyl)thio)acetic acid (PPH^{N}O^{C}S) (6). ^{1}H NMR (600 MHz, DMSO-d_6): δ_H 7.76 (bs, 2H, NH_3·TFA, H-1), 3.70 (t, *J* = 5.6 Hz, 2H, H-6), 3.56-3.62 (m, 8H, H-3, 5, 9, 11), 2.96 (s, 2H, H-2). **^{13}C NMR** (150 MHz, DMSO-d_6): δ_C 170.9 (C-8), 169.3 (C-12), 66.3 (C-3, 5), 46.9 (C-6), 38.6 (C-2), 32.6 (C-9, 11). **LRMS** (ESI+): *m/z* ([M+H]$^+$, 100%): 253.1. **HRMS**: *m/z:* [M+H]$^+$ calcd. for $C_8H_{17}N_2O_5S$: 253.08527; found: 253.08501.

Electronic supplementary information (ESI). Additional data for **1**–**6** (NMR spectroscopy, HRMS). See DOI:

Acknowledgments

This work was supported by the Australian Research Council (DP140100092) and the Australian Government Research Training Program (RTP) Scholarship scheme (C.J.M.B.). Mr A. Sresuthasan is acknowledged for useful discussions.

References

(1) Albrecht-Gary, A.-M.; Crumbliss, A. L. In *Metal Ions in Biological Systems*; Sigel, A., Sigel, H., Eds.; Marcel Dekker, Inc.: New York, 1998; Vol. 35, p 239–327.

(2) Butler, A. Iron acquisition: straight up and on the rocks? *Nat. Struct. Biol.*, **2003**, *10*, 240–241.

(3) Raymond, K. N.; Dertz, E. A. In *Iron Transport in Bacteria*; Crosa, J. H., Mey, A. R., Payne, S. M., Eds.; ASM Press: Washington, DC, 2004, p 3–17.

(4) Hider, R. C.; Kong, X. Chemistry and biology of siderophores. *Nat. Prod. Rep.*, **2010**, *27*, 637–657.

(5) Miethke, M. Molecular strategies of microbial iron assimilation: from high-affinity complexes to cofactor assembly systems. *Metallomics*, **2013**, *5*, 15–28.

(6) Sandy, M.; Butler, A. Microbial iron acquisition: Marine and terrestrial siderophores. *Chem. Rev.*, **2009**, *109*, 4580–4595.

(7) Chu, B. C.; Garcia-Herrero, A.; Johanson, T. H.; Krewulak, K. D.; Lau, C. K.; Peacock, R. S.; Slavinskaya, Z.; Vogel, H. J. Siderophore uptake in bacteria and the battle for iron with the host; a bird's eye view. *BioMetals*, **2010**, *23*, 601–611.

(8) Schalk, I. J.; Hannauer, M.; Braud, A. New roles for bacterial siderophores in metal transport and tolerance. *Environ. Microbiol.*, **2011**, *13*, 2844–2854.

(9) Codd, R.; Richardson-Sanchez, T.; Telfer, T. J.; Gotsbacher, M. P. Advances in the chemical biology of desferrioxamine B. *ACS Chem. Biol.*, **2018**, *13*, 11–25.

(10) Dhungana, S.; White, P. S.; Crumbliss, A. L. Crystal structure of ferrioxamine B: A comparative analysis and implications for molecular recognition. *J. Biol. Inorg. Chem.*, **2001**, *6*, 810–818.

(11) van der Helm, D.; Poling, M. The crystal structure of ferrioxamine E. *J. Am. Chem. Soc.*, **1976**, *98*, 82–86.

(12) Ledyard, K. M.; Butler, A. Structure of putrebactin, a new dihydroxamate siderophore produced by *Shewanella putrefaciens*. *J. Biol. Inorg. Chem.*, **1997**, *2*, 93–97.

(13) Böttcher, T.; Clardy, J. A chimeric siderophore halts swarming *Vibrio*. *Angew. Chem. Int. Ed.*, **2014**, *53*, 3510–3513.

(14) Soe, C. Z.; Pakchung, A. A. H.; Codd, R. Directing the biosynthesis of putrebactin or desferrioxamine B in *Shewanella putrefaciens* through the upstream inhibition of ornithine decarboxylase. *Chem. Biodivers.*, **2012**, *9*, 1880–1890.

(15) Winkelmann, G.; Schmid, D. G.; Nicholson, G.; Jung, G.; Colquhoun, D. J. Bisucaberin - a dihydroxamate siderophore isolated from *Vibrio salmonicida*, an important pathogen of farmed Atlantic salmon (*Salmo salar*). *BioMetals*, **2002**, *15*, 153–160.

(16) Soe, C. Z.; Telfer, T. J.; Levina, A.; Lay, P. A.; Codd, R. Simultaneous biosynthesis of putrebactin, avaroferrin and bisucaberin by *Shewanella putrefaciens* and characterisation of complexes with iron(III), molybdenum(VI) or chromium(V). *J. Inorg. Biochem.*, **2016**, *162*, 207–215.

(17) Takahashi, A.; Nakamura, H.; Kameyama, T.; Kurasawa, S.; Naganawa, H.; Okami, Y.; Takeuchi, T.; Umezawa, H. Bisucaberin, a new siderophore, sensitizing tumor cells to

macrophage-mediated cytolysis. II. Physico-chemical properties and structure determination. *J. Antibiot.*, **1987**, *40*, 1671–1676.

(18) Nishio, T.; Tanaka, N.; Hiratake, J.; Katsube, Y.; Ishida, Y.; Oda, J. Isolation and structure of the novel dihydroxamate siderophore alcaligin. *J. Am. Chem. Soc.*, **1988**, *110*, 8733–8734.

(19) Codd, R.; Soe, C. Z.; Pakchung, A. A. H.; Sresutharsan, A.; Brown, C. J. M.; Tieu, W. The chemical biology and coordinaton chemistry of putrebactin, avaroferrin, bisucaberin, and alcaligin. *J. Biol. Inorg. Chem.*, **2018**, *23*, 969–982.

(20) Pakchung, A. A. H.; Soe, C. Z.; Lifa, T.; Codd, R. Complexes formed in solution between vanadium(IV)/(V) and the cyclic dihydroxamic acid putrebactin or linear suberodihydroxamic acid. *Inorg. Chem.*, **2011**, *50*, 5978–5989.

(21) Soe, C. Z.; Pakchung, A. A. H.; Codd, R. Dinuclear $[V^{V}O(\text{putrebactin}))_2(\mu\text{-}OCH_3)_2]$ formed in solution as established from LC-MS measurements using ^{50}V-enriched V_2O_5. *Inorg. Chem.*, **2014**, *53*, 5852–5861.

(22) Bergeron, R. J.; McManis, J. S. The total synthesis of bisucaberin. *Tetrahedron*, **1989**, *45*, 4939–4944.

(23) Driggers, E. M.; Hale, S. P.; Lee, J.; Terrett, N. K. The exploration of macrocycles for drug discovery - an underexploited structural class. *Nat. Rev. Drug Discov.*, **2008**, *7*, 608–624.

(24) Giordanetto, F.; Kihlberg, J. Macrocyclic drugs and clinical candidates: What can medicinal chemists learn from their properties? *J. Med. Chem.*, **2014**, *57*, 278–295.

(25) Ardi, V. C.; Alexander, L. D.; Johnson, V. A.; McAlpine, S. R. Macrocycles that inhibit the binding between heat shock protein 90 and TPR-containing proteins. *ACS Chem. Biol.*, **2014**, *6*, 1357–1366.

(26) Marti-Centelles, V.; Pandey, M. D.; Burguete, M. I.; Luis, S. V. Macrocyclization reactions: the importance of conformational, configurational, and template-induced preorganisation. *Chem. Rev.*, **2015**, *115*, 8736–8834.

(27) Dougherty, P. G.; Qian, Z.; Pei, D. Macrocycles as protein-protein interaction inhibitors. *Biochem. J.*, **2017**, *474*, 1109–1125.

(28) Cummings, M. D.; Sekharan, S. Structure-based macrocycle design in small-molecule drug discovery and simple metrics to identify opportunities for macrocyclization of small-molecule ligands. *J. Med. Chem.*, **2019**, *DOI:10.1021/acs.jmedchem.8b01985*.

(29) Sresutharsan, A.; Tieu, W.; Richardson-Sanchez, T.; Soe, C. Z.; Codd, R. Dimeric and trimeric homo- and heteroleptic hydroxamic acid macrocycles formed using mixed-ligand Fe(III)-based metal-templated synthesis. *J. Inorg. Biochem.*, **2017**, *177*, 344–351.

(30) Kachadourian, R.; Chuilon, S.; Mérienne, C.; Kunesch, G.; Deroussent, A. A new total synthesis of ferrioxamine E through metal-templated cyclic trimerization. *Supramol. Chem.*, **1997**, *8*, 301–308.

(31) Lifa, T.; Tieu, W.; Hocking, R. K.; Codd, R. Forward and reverse (*retro*) iron(III)- or gallium(III)-desferrioxamine E and ring-expanded analogs prepared using metal-templated synthesis from *endo*-hydroxamic acid monomers. *Inorg. Chem.*, **2015**, *54*, 3573–3583.

(32) Tieu, W.; Lifa, T.; Katsifis, A.; Codd, R. Octadentate zirconium(IV)-loaded macrocycles with varied stoichiometry assembled from hydroxamic acid monomers using metal-templated synthesis. *Inorg. Chem.*, **2017**, *56*, 3719–3728.

(33) Wencewicz, T. A.; Oliver, A. G.; Miller, M. J. Iron(III)-templated macrolactonization of trihydroxamate siderophores. *Org. Lett.*, **2012**, *14*, 4390–4393.

(34) Holland, J. P.; Divilov, V.; Bander, N. H.; Smith-Jones, P. M.; Larson, S. M.; Lewis, J. S. ^{89}Zr-DFO-J591 for immunoPET of prostate-specific membrane antigen expression *in vivo*. *J. Nucl. Med.*, **2010**, *51*, 1293–1300.

(35) Holland, J. P.; Vasdev, N. Charting the mechanism and reactivity of zirconium oxalate with hydroxamate ligands using density functional theory: Implications in new chelate design. *Dalton Trans.*, **2014**, *43*, 9872–9884.

(36) Bergeron, R. J.; Liu, Z.-R.; McManis, J. S.; Wiegand, J. Structural alterations in desferrioxamine compatible with iron clearance in animals. *J. Med. Chem.*, **1992**, *35*, 4739–4744.

(37) Kadi, N.; Oves-Costales, D.; Barona-Gómez, F.; Challis, G. L. A new family of ATP-dependent oligomerization-macrocyclization biocatalysts. *Nat. Chem. Biol.*, **2007**, *3*, 652–656.

(38) Izawa, T.; Mukaiyama, T. The partial reduction of carboxylic acids to aldehydes *via* 3-acylthiazolidine-2-thiones with diisobutylaluminum hydride and with lithium tri-tert-butoxyaluminum hydride. *Bull. Chem. Soc. Jpn.*, **1979**, *52*, 555–558.

(39) Bergeron, R. J.; Pegram, J. J. An efficient total synthesis of desferrioxamine B. *J. Org. Chem.*, **1988**, *53*, 3131–3134.

(40) Rütschlin, S.; Böttcher, T. Dissecting the mechanism of oligomerization and macrocyclization reactions of NRPS-independent siderophore synthetases. *Chem. Eur. J.*, **2018**, *24*, 16044–16051.

(41) Reddy, P. A.; Schall, O. F.; Wheatley, J. R.; Rosik, L. O.; McClurg, J. P.; Marshall, G. R.; Slomczynska, U. *O*-Protected *N*-(2-nitrophenylsulfonyl)hydroxylamines: Novel reagents for the synthesis of hydroxamates. *Synthesis*, **2001**, 1086–1092.

(42) Poreddy, A. R.; Schall, O. F.; Osiek, T. A.; Wheatley, J. R.; Beusen, D. D.; Marshall, G. R.; Slomczynska, U. Hydroxamate-based iron chelators: Combinatorial syntheses of desferrioxamine B analogues and evaluation of binding affinities. *J. Comb. Chem.*, **2004**, *6*, 239–254.

(43) Price, E. W.; Zeglis, B. M.; Cawthray, J. F.; Lewis, J. S.; Adam, M. J.; Orvig, C. What a difference a carbon makes: H_4octapa vs H_4C3octapa, ligands for In-111 and Lu-177 radiochemistry. *Inorg. Chem.*, **2014**, *53*, 10412–10431.

(44) Shioiri, T.; Ninomiya, K.; Yamada, S. Diphenylphosphoryl azide. A new convenient reagent for a modified Curtus reaction and for the peptide synthesis. *J. Am. Chem. Soc.*, **1972**, *94*, 6203–6205.

(45) Montalbetti, C. A. G. N.; Falque, V. Amide bond formation and peptide coupling. *Tetrahedron*, **2005**, *61*, 10827–10852.

(46) Kurth, C.; Kage, H.; Nett, M. Siderophores as molecular tools in medical and environmental applications. *Org. Biomol. Chem.*, **2016**, *14*, 8212–8227.

(47) Johnstone, T. C.; Nolan, E. M. Beyond iron: non-classical biological functions of bacterial siderophores. *Dalton Trans.*, **2015**, *44*, 6320–6339.

(48) Szabo, M.; Klein Herenbrink, C.; Christopoulos, A.; Lane, J. R.; Capuano, B. Structure-activity relationships of privileged structures lead to the discovery of novel biased ligands at the dopamine D2 receptor. *J. Med. Chem.*, **2014**, *57*, 4924–4939.

(49) Singh, V.; Wang, S.; Kool, E. T. Genetically encoded multispectral labeling of proteins with polyfluorophores on a DNA backbone. *J. Am. Chem. Soc.*, **2013**, *135*, 6184–6191.

ToC Graphic

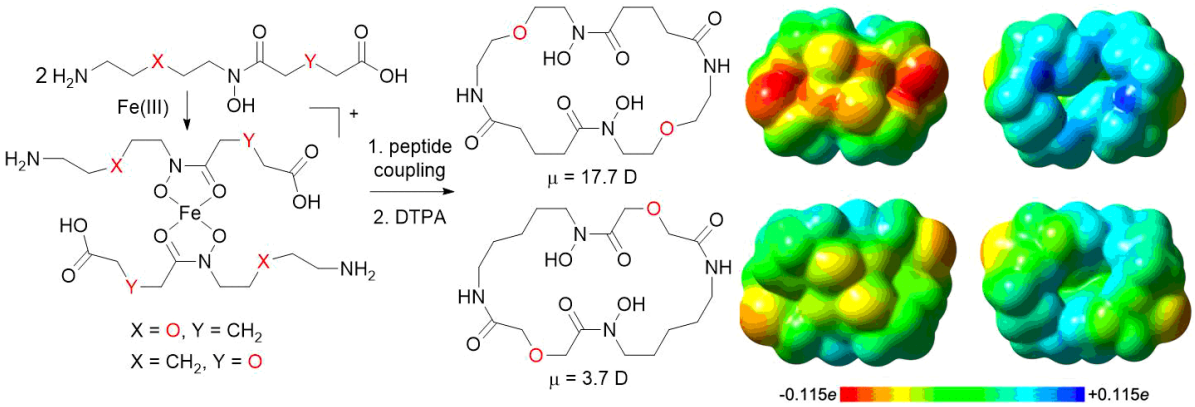
2 H2N
X
N
OH
Y
O
OH
Fe(III)
+
H2N
X
N
Y
O
OH
Fe
HO
O
N
X
NH2
Y
X = O, Y = CH2
X = CH2, Y = O
1. peptide coupling
2. DTPA
HO
N
O
NH
HN
O
OH
μ = 17.7 D
μ = 3.7 D
-0.115e
+0.115e